A gradual decrease in motion artifact was observed over a few minutes after the subject sat on the chair, which may have been caused by the increase in moisture in clothes due to sweating. Furthermore, a decrease in noise level was observed when the moisture in clothes increased. These observations show the notable influence of moisture on the measurement necessitating further study on the effects of humidity.

Though the signal quality obtained was poorer than that obtained using conventional methods, the presented ECG measurement method has the substantial advantage of being easily used on a daily basis. The method can be used for daily ECG monitoring as an auxiliary diagnostic device, or for a long-term HRV measurement.

VI. Conclusion

We described a method of taking ECG measurements that does not rely on direct skin contact. The method utilizes high-input-impedance active electrodes and indirect-contact grounding. The signal quality of the presented method was lower than those of conventional methods and was dependent on clothing properties. However, our results demonstrate the potential of this technique for long-term, convenient, everyday use.

References

[1] M. Ogawa and T. Togawa, "Attempts at monitoring health status in the home," in *Proc. 1st Annu. Int. IEEE-EMBS Special Topic Conf. Microtechnologies in Medicine & Biology*, 2000, pp. 552–556.

[2] M. Ishijima, "Monitoring of electrocardiograms in bed without utilizing body surface electrodes," *IEEE Trans. Biomed. Eng.*, vol. 40, no. 6, pp. 593–594, Jun. 1993.

[3] T. Tamura, T. Togawa, M. Ogawa, and M. Yoda, "Fully automated health monitoring system in the home," *Med. Eng. Phys.*, vol. 20, pp. 573–579, 1998.

[4] C. J. Harland, T. D. Clark, and R. J. Prance, "Electric potential probes-new directions in the remote sensing of the human body," *Meas. Sci. Technol.*, vol. 13, pp. 163–169, 2002.

[5] H. W. Ott, *Noise Reduction Techniques in Electronic Systems*, 2nd ed. New York: Wiley, 1988, pp. 244–273.

[6] *Diagnostic Electrocardiographic Devices*, ANSI Standard ANSI/AAMI EC11-1991.

Linear Minimum Mean-Square Error Filtering for Evoked Responses: Application to Fetal MEG

Mingli Chen, Barry D. Van Veen, and Ronald T. Wakai*

***Abstract*—This paper describes a linear minimum mean-squared error (LMMSE) approach for designing spatial filters that improve the signal-to-noise ratio (SNR) of multiepoch evoked response data. This approach does not rely on availability of a forward solution and thus is applicable to problems in which a forward solution is not readily available, such as fetal magnetoencephalography (fMEG). The LMMSE criterion leads to a spatial filter that is a function of the autocorrelation matrix of the data and the autocorrelation matrix of the signal. The signal statistics are unknown, so we approximate the signal autocorrelation matrix using the average of the data across epochs. This approximation is reasonable provided the mean of the noise is zero across epochs and the signal mean is significant. An analysis of the error incurred using this approximation is presented. Calculations of SNR for the exact and approximate LMMSE filters and simple averaging for the rank-1 signal case are shown. The effectiveness of the method is demonstrated with simulated evoked response data and fetal MEG data.**

***Index Terms*—Linear minimum mean square error (LMMSE), magnetoencephalography (MEG), spatial filter.**

I. Introduction

The most common method of increasing the signal-to-noise ratio (SNR) of evoked response data is averaging; however, this simplistic approach is often inadequate when the number of trials and/or the SNR is low, which is often the case for magnetoencephalography (MEG) and electroencephalography (EEG) signals. An extreme example of a low SNR signal is the fetal magnetoencephalogram (fMEG) [1]–[3]. In the last few years, MEG has been increasingly utilized to study the development of brain activity in the fetus, as well as the neonate. Fetal recordings are arguably the most difficult of all MEG signals to record due to their very low amplitude and the presence of strong cardiac interference from both the fetus and mother.

Recent attempts to improve the SNR of the fMEG have centered on spatial filtering techniques [4], [5]. MEG recording systems typically allow for acquisition of many channels, and the sensor covariance exhibits considerable spatial structure, which can be exploited with suitable signal processing techniques. Many spatial filtering methods, such as linearly constrained minimum variance spatial filtering [6], require knowledge of the forward solution; however, this is problematic for fMEG due to the lack of a simple, accurate source model. In the absence of a forward solution, more general methods such as principle component analysis (PCA) and maximum-likelihood estimation (MLE) [7] can still be employed. PCA exploits the low-rank spatial structure of the signal, but requires rank determination and whitening to be effective [8]. MLE exploits low-rank spatio-temporal structure and inherently accommodates spatially colored noise, but also requires rank determination.

Manuscript received May 2, 2005; revised October 1, 2005. This work was supported by the National Institute of Health (NIH) under Grant R-01NS37740. *Asterisk indictaes corresponding author.*

M. Chen is with the Department of Medical Physics, University of Wisconsin-Madison, Madison, WI 53706 USA (e-mail: mlchen@wisc.edu).

B. D. Van Veen is with the Department of Electrical and Computer Engineering, University of Wisconsin-Madison, Madison, WI 53706 USA (e-mail: vanveen@engr.wisc.edu).

*R. T. Wakai is with the Department of Medical Physics, University of Wisconsin-Madison, Madison, WI 53706 USA (e-mail: rtwakai@wisc.edu).

Digital Object Identifier 10.1109/TBME.2006.872822

In this paper, we formulate a linear minimum mean-square error (LMMSE) filter and show that it can significantly improve the SNR of fetal auditory evoked response (fAER) data. The filter does not require a forward solution or rank determination and is applicable to spatially colored noise. Several variations of LMMSE filtering have been previously applied to evoked potential data [9], [10], often for estimation of single-trial evoked responses. Our LMMSE filter differs from prior ones in the way in which the signal is approximated and the correlation matrices are estimated. In Section II, we describe the formulation of the filter, including estimation of the signal statistics. In Section III, we compute the excess mean square error of our approximate solution with respect to the true solution and compare the SNR of our method to that of the exact LMMSE filter and averaging. Simulated and real fMEG data show that our LMMSE filter can be effective even in very low SNR situations. Although here we only consider fMEG data, the filter can be applied to virtually any multiepoch evoked response data, including EEG data.

Bold face upper and lower case fonts are used to denote matrices and vectors, respectively. Superscripts t and -1 denote matrix transpose and matrix inverse. The expectation of a random vector or a matrix is denoted by $\langle\ \rangle$. The covariance of a matrix $\mathbf{A}$ is defined as $\mathbf{C_A} = \langle(\mathbf{A}-\langle\mathbf{A}\rangle)(\mathbf{A}-\langle\mathbf{A}\rangle)^t\rangle$ and the trace of a square matrix $\mathbf{A}$ is denoted by $tr\{\mathbf{A}\}$.

II. Methods

Let $\mathbf{X}$ denote a $n \times T$ data matrix representing a single trial, where n is the number of channels and T is the number of samples in each trial. Suppose $\mathbf{S}$ and $\mathbf{N}$ denote the signal and noise, respectively, so $\mathbf{X} = \mathbf{S} + \mathbf{N}$. The method presented here assumes the signal has a significant mean component, the noise has zero mean, and the signal and noise are uncorrelated, i.e. $\langle\mathbf{S}\rangle \neq \mathbf{0}$, $\langle\mathbf{N}\rangle = \mathbf{0}$ and $\langle\mathbf{S}\mathbf{N}^t\rangle = \mathbf{0}$.

Define the mean-square error (MSE) between the signal and the spatial filter, $\mathbf{F}$, applied to the data as

$$e^2(\mathbf{F}) = tr\left\langle(\mathbf{S}-\mathbf{F}\mathbf{X})(\mathbf{S}-\mathbf{F}\mathbf{X})^t\right\rangle. \tag{1}$$

The filter that minimizes $e^2(\mathbf{F})$ is given by $\mathbf{F} = \mathbf{F}_{\min} = \mathbf{R_{SS}}\mathbf{R_{XX}^{-1}}$, where $\mathbf{R_{SS}} = \langle\mathbf{S}\mathbf{S}^t\rangle$ and $\mathbf{R_{XX}} = \langle\mathbf{X}\mathbf{X}^t\rangle$ (See [11]). The minimum MSE is

$$e^2_{\min} = tr\left\{\mathbf{R_{SS}} - \mathbf{R_{SS}}\mathbf{R_{XX}^{-1}}\mathbf{R_{SS}}\right\}. \tag{2}$$

In practice, $\mathbf{R_{SS}}$ and $\mathbf{R_{XX}}$ are not available and must be approximated using the data.

Let $\mathbf{X}_1, \mathbf{X}_2, \ldots, \mathbf{X}_J$ denote J independent trials in a multiepoch recording and assume $\mathbf{X}_i = \mathbf{S}_i + \mathbf{N}_i$. It is straightforward to approximate $\mathbf{R_{XX}}$ using the sample average

$$\hat{\mathbf{R}}_{\mathbf{XX}} = \frac{1}{J}\sum_{i=1}^{J}\mathbf{X}_i\mathbf{X}_i^t. \tag{3}$$

For J large enough, we have $\hat{\mathbf{R}}_{\mathbf{XX}} \rightarrow \mathbf{R_{XX}}$. We exploit the mean of the signal and noise to approximate $\mathbf{R_{SS}}$ as

$$\hat{\mathbf{R}}_{\mathbf{SS}} = \mathbf{X}_{\text{ave}}\mathbf{X}_{\text{ave}}^t, \tag{4}$$

where $\mathbf{X}_{\text{ave}} = (1/J)\sum_{i=1}^{J}\mathbf{X}_i$. The mean of $\hat{\mathbf{R}}_{\mathbf{SS}}$ is

$$\langle\hat{\mathbf{R}}_{\mathbf{SS}}\rangle = \bar{\mathbf{S}}\bar{\mathbf{S}}^t + \frac{1}{J}\mathbf{C_S} + \frac{1}{J}\mathbf{C_N} \tag{5}$$

where $\bar{\mathbf{S}} = \langle\mathbf{S}\rangle$. Note that $\hat{\mathbf{R}}_{\mathbf{SS}}$ is biased since the quantity we seek to approximate is $\mathbf{R_{SS}} = \bar{\mathbf{S}}\bar{\mathbf{S}}^t + \mathbf{C_S}$.

III. Performance Analysis

We now study the performance obtained using $\mathbf{F}_{\min}$, $\hat{\mathbf{F}} = \hat{\mathbf{R}}_{\mathbf{SS}}\hat{\mathbf{R}}_{\mathbf{XX}}^{-1}$, and simple averaging. The excess MSE, $e^2_{ex}(\mathbf{F}) = e^2(\mathbf{F}) - e^2_{\min}$ can be expressed as

$$e^2_{ex}(\mathbf{F}) = tr\left\{\left(\mathbf{F}-\mathbf{R_{SS}}\mathbf{R_{XX}^{-1}}\right)\mathbf{R_{XX}}\left(\mathbf{F}-\mathbf{R_{SS}}\mathbf{R_{XX}^{-1}}\right)^t\right\}. \tag{6}$$

For this analysis we assume that J is sufficiently large so that $\hat{\mathbf{R}}_{\mathbf{SS}}$ and $\hat{\mathbf{R}}_{\mathbf{XX}}$ approach $\langle\hat{\mathbf{R}}_{\mathbf{SS}}\rangle$ and $\mathbf{R_{XX}}$, respectively, and thus use $\mathbf{F}_{\text{app}} = \langle\hat{\mathbf{R}}_{\mathbf{SS}}\rangle\mathbf{R_{XX}^{-1}}$ to compute the excess MSE in place of $\hat{\mathbf{F}}$. This yields

$$e^2_{ex}(\mathbf{F}_{\text{app}}) = tr\left\{\left(\frac{J-1}{J}\mathbf{C_S} - \frac{1}{J}\mathbf{C_N}\right) \times \mathbf{R_{XX}^{-1}}\left(\frac{J-1}{J}\mathbf{C_S} - \frac{1}{J}\mathbf{C_N}\right)^t\right\} \tag{7}$$

which suggests $e^2_{ex}(\mathbf{F}_{\text{app}})$ decreases as $\mathbf{C_S}$ decreases and J increases.

We further consider the performance of $\mathbf{F}_{\text{app}}$ for the specific case of a rank-one signal $\mathbf{S} = \mathbf{h}\boldsymbol{\alpha}^t$, where $\mathbf{h}$ is an $n \times 1$ spatial pattern and $\boldsymbol{\alpha}$ is a $T \times 1$ random vector describing the time evolution of the signal. We assume $\mathbf{h}^t\mathbf{h} = 1$ and define $\bar{\boldsymbol{\alpha}} = \langle\boldsymbol{\alpha}\rangle$, $\sigma^2 = \langle(\boldsymbol{\alpha}-\bar{\boldsymbol{\alpha}})^t(\boldsymbol{\alpha}-\bar{\boldsymbol{\alpha}})\rangle$, and $\beta = \bar{\boldsymbol{\alpha}}^t\bar{\boldsymbol{\alpha}} + \sigma^2$. Note that with these definitions $\mathbf{R_{XX}} = \beta\mathbf{h}\mathbf{h}^t + \mathbf{C_N}$ and thus $\mathbf{R_{XX}^{-1}}$ can be computed in closed form via the matrix inversion lemma.

We use the SNR of the estimated mean signal, $\hat{\bar{\mathbf{S}}} = \mathbf{F}\mathbf{X}_{\text{ave}}$, as a performance metric. First, note that

$$\mathbf{F}_{\min}\mathbf{X}_{\text{ave}} = \mathbf{R_{SS}}\mathbf{R_{XX}^{-1}}\left(\bar{\mathbf{S}} + \frac{1}{J}\sum_{i=1}^{J}(\mathbf{S}_i - \bar{\mathbf{S}}) + \frac{1}{J}\sum_{i=1}^{J}\mathbf{N}_i\right). \tag{8}$$

The power in $\mathbf{F}_{\min}\mathbf{X}_{\text{ave}}$ due to the signal is defined as

$$SP(\mathbf{F}_{\min}\mathbf{X}_{\text{ave}}) = tr\left\{\mathbf{R_{SS}}\mathbf{R_{XX}^{-1}}\left\langle\left(\bar{\mathbf{S}} + \frac{1}{J}\sum_{i=1}^{J}(\mathbf{S}_i - \bar{\mathbf{S}})\right) \times \left(\bar{\mathbf{S}} + \frac{1}{J}\sum_{i=1}^{J}(\mathbf{S}_i - \bar{\mathbf{S}})\right)^t\right\rangle\mathbf{R_{XX}^{-1}}\mathbf{R_{SS}}\right\}. \tag{9}$$

After simplification (9) becomes

$$SP(\mathbf{F}_{\min}\mathbf{X}_{\text{ave}}) = \beta^2\gamma\left(\frac{\nu}{1+\beta\nu}\right)^2 \tag{10}$$

where $\gamma = \bar{\boldsymbol{\alpha}}^t\bar{\boldsymbol{\alpha}} + (1/J)\sigma^2$ and $\nu = \mathbf{h}^t\mathbf{C_N^{-1}}\mathbf{h}$. The noise power $\text{NP}(\mathbf{F}_{\min}\mathbf{X}_{\text{ave}})$ in $\mathbf{F}_{\min}\mathbf{X}_{\text{ave}}$ is defined similarly to obtain

$$\text{NP}(\mathbf{F}_{\min}\mathbf{X}_{\text{ave}}) = \frac{1}{J}\beta^2\frac{\nu}{(1+\beta\nu)^2}. \tag{11}$$

Hence, the SNR of $\mathbf{F}_{\min}\mathbf{X}_{\text{ave}}$ is the ratio of (10) to (11) which is

$$\text{SNR}(\mathbf{F}_{\min}\mathbf{X}_{\text{ave}}) = J\gamma\nu. \tag{12}$$

For comparison, the SNR of the mean in the absence of spatial filtering ($\mathbf{F} = \mathbf{I}$) is

$$\text{SNR}(\mathbf{X}_{\text{ave}}) = \frac{J\gamma}{tr\{\mathbf{C_N}\}}. \tag{13}$$

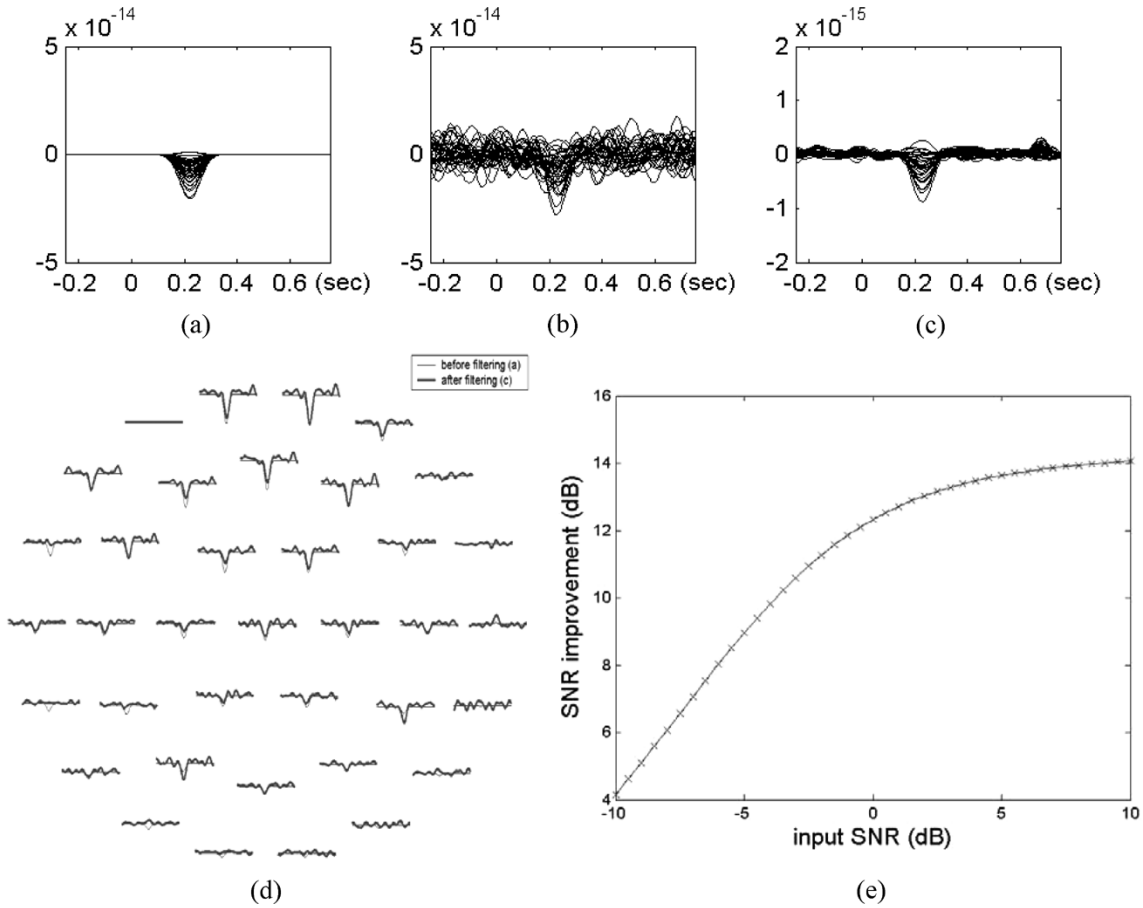

Fig. 1. Simulation results for Gaussian noise. (a)–(c) Superposition plots of 37-channel data: (a) noise-free synthetic signal, (b) the signal obtained by averaging, and (c) LMMSE filter output. (d) Sensor layout plot of 37-channel data, showing the spatial pattern of the signal before and after filtering. (e) SNR improvement attained by the filter versus SNR of the filter input, obtained by averaging. The results in (a)–(d) are for an input SNR of -5 dB.

The ratio of the optimum spatial filter SNR (12) to the SNR without spatial filtering (13) is

$$\frac{\mathrm{SNR}(\mathbf{F}_{\min}\mathbf{X}_{\mathrm{ave}})}{\mathrm{SNR}(\mathbf{X}_{\mathrm{ave}})} = \nu \cdot tr\{\mathbf{C_N}\}. \tag{14}$$

It can be shown that (14) is greater than one, so the optimum spatial filter always improves SNR.

It can be shown that the SNR of $\mathbf{F}_{\mathrm{app}}\mathbf{X}_{\mathrm{ave}}$ is

$$\mathrm{SNR}(\mathbf{F}_{\mathrm{app}}\mathbf{X}_{\mathrm{ave}}) = \frac{\gamma\left(\gamma+\frac{1}{J}\nu^{-1}\right)^2\nu^2}{\frac{1}{J}\gamma^2\nu+\frac{1}{J^2}2\gamma(1+\beta\nu)+\frac{1}{J^3}\left(tr\{\mathbf{C_N}\}-\frac{2\beta+\beta^2\nu}{1+\beta\nu}\right)(1+\beta\nu)^2}. \tag{15}$$

The ratio of (15) over (13) is

$$\frac{\mathrm{SNR}(\mathbf{F}_{\mathrm{app}}\mathbf{X}_{\mathrm{ave}})}{\mathrm{SNR}(\mathbf{X}_{\mathrm{ave}})} = \frac{\gamma\left(\gamma+\frac{1}{J}\nu^{-1}\right)^2\nu^2\cdot tr\{\mathbf{C_N}\}}{\gamma\left(\gamma^2\nu+\frac{1}{J}2\gamma(1+\beta\nu)+\frac{1}{J^2}\left(tr\{\mathbf{C_N}\}-\frac{2\beta+\beta^2\nu}{1+\beta\nu}\right)(1+\beta\nu)^2\right)}. \tag{16}$$

As $J \to \infty$, (16) approaches (14). Thus, $\mathbf{F}_{\mathrm{app}}$ improves the SNR relative to averaging provided J is sufficiently large.

IV. Experiments

The performance of the algorithm was evaluated by applying it to fAER data and to two types of simulated data. The purpose of the simulations was to quantify the improvement in SNR and to assess the distortion of the spatial pattern introduced by the filter.

The simulated data were obtained by embedding multiple occurrences of a synthetic signal in noise. The time-evolution of the synthetic signal, which was designed to mimic a fAER, was a Gaussian pulse with full width at half maximum of 91 ms. The spatial pattern was obtained by computing the forward solution for a current dipole in a sphere, adjusting the dipole position and orientation to produce a signal pattern of a typical dipolar source beneath the sensor [Figs. 1(d) and 2(d)]. The use of such a low-rank signal is appropriate for fetal sources, which generally are dipolar because their physical dimensions typically are much less than the source-to-sensor distance. SNR was adjusted by varying the amplitude of the synthetic signal. For the first set of simulations, the noise was an artificially generated white Gaussian noise time-series. A run of 400 trials was simulated by adding the synthetic signal to 400 1-s epochs of noise, with the peak of the synthetic signal positioned at time 0.22 s.

For the second set of simulations, the noise consisted of recordings taken from a fetus in the absence of auditory stimulation, obtained using the following procedure. A 37-channel biomagnetometer (Magnes, 4D Neuroimaging) was placed over the abdomen of a pregnant mother, near the location of the fetal scalp. A ten-minute recording with 0.1–200 Hz passband and 520 Hz sampling rate was acquired in

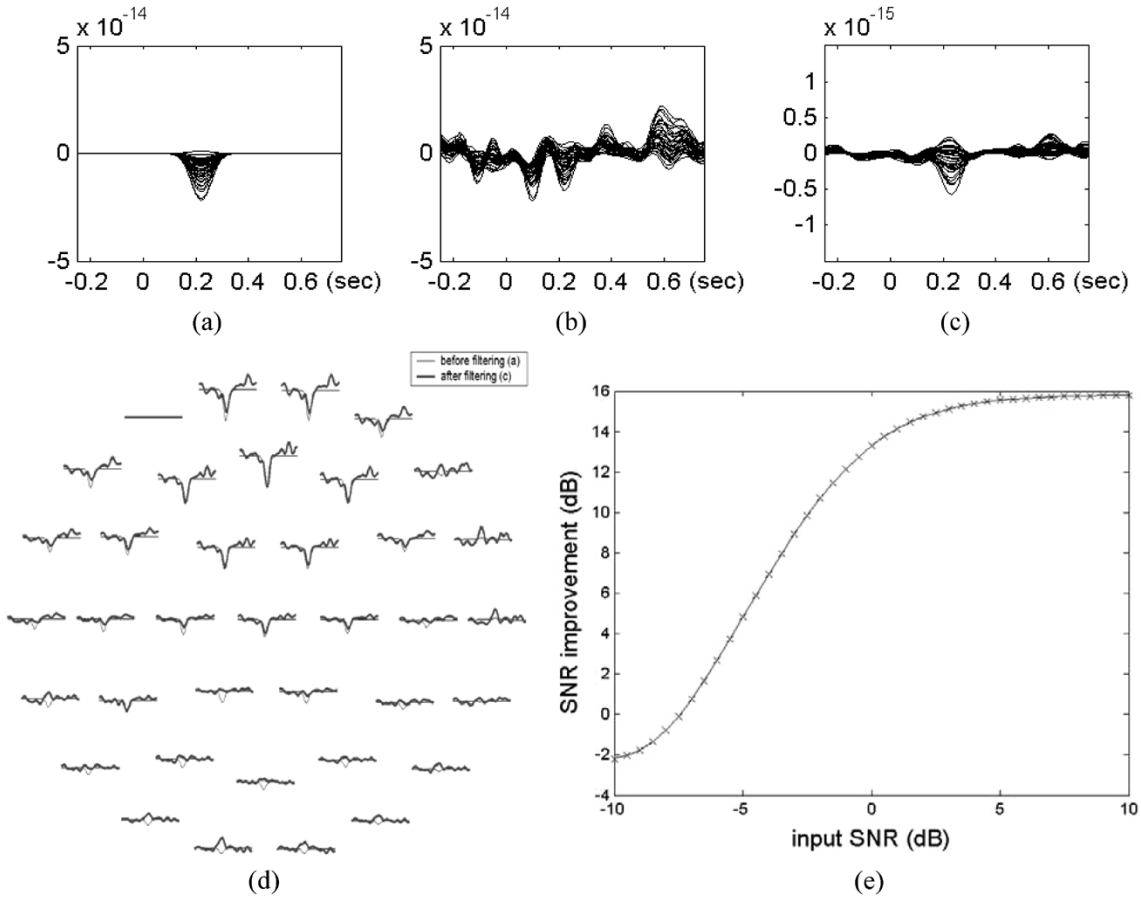

Fig. 2. Simulation results for recorded noise. (a)–(c) Superposition plots of 37-channel data: (a) noise-free synthetic signal, (b) the signal obtained by averaging, and (c) LMMSE filter output. (d) Sensor layout plot of 37-channel data, showing the spatial pattern of the signal before and after filtering. (e) SNR improvement attained by the filter versus SNR of the filter input, obtained by averaging. The results in (a)–(d) are for an input SNR of -5 dB.

the absence of auditory stimulation. This recording contained the interferences typically encountered in fMEG recordings—fetal magnetocardiography (MCG), maternal MCG, and other biological interference, such as maternal and fetal breathing and body movement artifact, as well as environmental and instrumental interference. Four hundred occurrences of the synthetic signal were added to the recordings with random 1–2 s interval to prevent synchronization with periodic interference. The signal was digitally filtered with passband 0.5–10 Hz and parsed into 400 1-s epochs, each beginning 0.25 s prior to the onset of the signal. Cardiac interference is not removed. Artifact rejection was performed using an amplitude threshold of 2.5×10^{-12} T; however, no epochs were rejected.

The simulation results for white Gaussian noise are presented in Fig. 1. Fig. 1(a)–(c) shows the result of one simulation: Fig. 1(a) is the noise-free synthetic signal, Fig. 1(b) is the signal obtained by averaging, and Fig. 1(c) is the LMMSE filter output. Fig. 1(d) shows the spatial pattern of the signal before and after filtering. The results of 41 simulations are summarized in Fig. 1(e), using (13) and (15) to compute the SNR improvement attained by the filter versus SNR of the filter input, obtained by averaging. The simulation results for recorded noise are presented in Fig. 2, following the same format as Fig. 1.

Next, fAER data was collected from a normal fetus at gestational age 37 weeks using 300 auditory tone bursts of frequency 1.5 kHz, intensity 100 dB, and duration 100 ms. The tone bursts were presented at random 1–2 s intervals during the 450 s recording period. Two data collection sessions were performed. After applying a 0.5–10 Hz bandpass filter and performing artifact rejection using a 2000 fT amplitude threshold, 255 and 287 trials were available for analysis. Averaged fAERs from runs 1 and 2, respectively, are shown in Fig. 3(a) and (c); the results of LMMSE filtering are shown in Fig. 3(b) and (d). The signal was visible after averaging in the first run [Fig. 3(a)], but contained significant interference which was removed by the LMMSE filter [Fig. 3(b)]. In the second run, the signal was difficult to identify after averaging [Fig. 3(c)], whereas the LMMSE filter yielded a signal [Fig. 3(d)] with morphology and spatial pattern similar to that obtained in the first run. The signal latencies were consistent with those reported in previous fAER studies [1]–[3].

V. Discussion

The LMMSE filter can significantly increase the SNR of fAER recordings, improving the resolution of weak signals that are obscured by noise even after averaging. This approach is well suited for fMEG because the assumptions are minimal and no user input concerning desired signal characteristics is required. Also, it is very effective at removing large interference, including fetal and maternal MCG. Other approaches for removing fetal and maternal MCG, such as matched filtering, have significant limitations.

The LMMSE filter generally produces signal amplitudes much smaller than those of the true signal. The fact that the procedure yields a biased estimate may account in part for why LMMSE methods are not more widely used. However, amplitude is of secondary importance for detection of the fAER—SNR is the most important criterion.

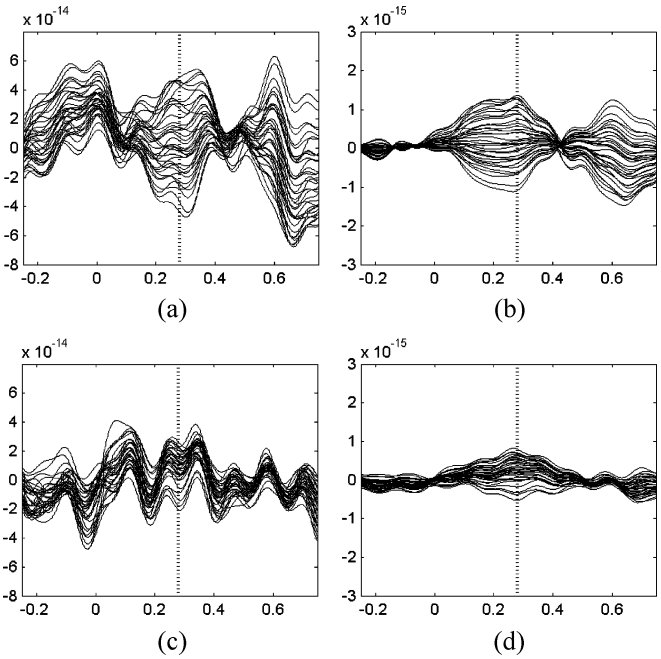

Fig 3. (a), (c) Averaged fetal auditory evoked responses for runs 1 and 2, respectively. (b), (d) LMMSE filter output for runs 1 and 2, respectively. Each window is 1 s long with prestimulus interval 250 ms and poststimulus interval 750 ms. The filtered signals show similar latency; the smaller amplitude in run 2 can be due to a number of causes such as fetal movement or state change.

Signal topography is also an important characteristic, and the distortion resulting from the LMMSE filter is modest.

REFERENCES

[1] J. Lengle, M. Chen, and R. Wakai, "Improved neuromagnetic detection of fetal and neonatal auditory evoked responses," *Clin. Neurophysiol.*, vol. 112, pp. 785–792, 2001.

[2] H. Eswaran, H. Preißl, J. D. Wilson, P. Murphy, S. E. Robinson, D. Rose, J. Vrba, and C. Lowery, "Short-term serial magnetoencephalography recordings of fetal auditory evoked responses," *Neurosci. Lett.*, vol. 331, pp. 128–132, 2002.

[3] U. Schneider, E. Schleussner, J. Haueisen, H. Nowak, and H. J. Seewald, "Signal analysis of auditory evoked cortical fields in fetal magnetoencephalography," *Brain Topogr.*, vol. 14, no. 1, pp. 69–80, 2001.

[4] S. E. Robinson, J. Vrba, and J. McCubbin *et al.*, "Separating fetal MEG signals from the noise," Biomag. 2002 H. Nowak, Ed. *et al.* Berlin, Germany, VDE Verlag GmbH, 2002, pp. 665–667.

[5] M. Chen, R. T. Wakai, and B. VanVeen, "Eigen-vector based spatial filtering of fetal biomagnetic signals," *J. Perinat. Med.*, vol. 29, pp. 486–496, 2001.

[6] B. D. Van Veen, W. van Drongelen, M. Yuchtman, and A. Suzuki, "Localization of brain electrical activity via linearly constrained minimum variance spatial filtering," *IEEE Trans. Biomed. Eng.*, vol. 44, no. 9, pp. 867–880, Sep. 1997.

[7] B. V. Baryshnikov, B. D. Van Veen, and R. T. Wakai, "Maximum-likelihood estimation of low-rank signals for multiepoch MEG/EEG analysis," *IEEE Trans. Biomed. Eng.*, vol. 51, no. 11, pp. 1981–1993, Nov. 2004.

[8] K. Sekihara, D. Poeppel, A. Marantz, H. Koizumi, and Y. Miyashita, "MEG spatio-temporal analysis using a covariance matrix calculated from nonaveraged multiple-epoch data," *IEEE Trans. Biomed. Eng.*, vol. 46, no. 5, pp. 515–521, May 1999.

[9] K.-B. Yu and C. D. Mc Gillem, "Optimum filters for estimating evoked potential waveforms," *IEEE Trans. Biomed. Eng.*, vol. BME-30, pp. 730–737, 1983.

[10] J. J. Westerkamp and J. I. Aunon, "Optimum multielectrode a posteriori estimates of single-response evoked potentials," *IEEE Trans. Biomed. Eng.*, vol. BME-34, pp. 13–22, 1987.

[11] S. J. Orfanidis, *Optimum Signal Processing, An Introduction.* New York: Macmillan, 1985.

Evaluation of MRI RF Probes Utilizing Infrared Sensors

Tamer S. Ibrahim* and Robert Lee

***Abstract*—The magnetic resonance imaging (MRI) coil's radio frequency (RF) field distribution has a strong effect on image quality as well as specific absorption rate. In this paper, a method of probing a coil's RF field distribution over any unoccupied region of the coil is presented. This technique is based on the use of infrared sensing. The proposed method was implemented and tested on a high field RF volume coil operating at 340 MHz. Very good agreement was achieved between the infrared measurements and numerical data obtained utilizing an in-house three-dimensional finite-difference time-domain package. The results demonstrate that the proposed technique is practical, robust, and efficient in making accurate measurements of the electric field distributions in loaded and unloaded MRI coils.**

***Index Terms*—FDTD, infrared sensors, RF coils.**

I. INTRODUCTION

The uniformity of magnetic resonance imaging (MRI) transmit and receive radio frequency (RF) fields greatly influences the image quality. As human MRI is now performed at field strengths reaching 7, 8, and 9.4 tesla (T), there is significant deterioration in the image quality due to the nonuniformity of the RF fields associated with such field strengths. This limits the usefulness of ultra high field ($\geq$7 T) human imaging. Although computational electromagnetics can be used to predict these fields [1]–[6] and is a vital tool in designing the RF probes [7], [8], experimental measurements of the RF fields are still necessary for validating the computational predictions and for confirming the performance of the RF probes.

Several researchers have developed methods for measuring the transmit field [9]–[12] as well as temperature changes due to RF absorption [13]–[15], however, obtaining rapid and accurate data over the coil's entire working volume remains a challenge. Scanning the coil with a field probe causes unavoidable perturbations in the field, most especially for ultra high field imaging frequencies, and it is extremely time consuming. Imaging techniques based on homogeneous phantoms [9] and thermochromic films embedded in phantoms [16] are effective for sensing fields over the region occupied by the phantom, but they provide no information about the fields outside of the phantom. In particular, a coil's radiation losses, which are essential in confirming specific absorption rate (SAR) predictions, cannot be measured with these imaging methods.

In this paper, we present a method of probing the field distribution over any unoccupied region of a coil. The technique is adapted from a previously used method for measurements of fields and current distributions in other applications (e.g., [17] and [18]). The method involves placing a very thin low-loss dielectric film into the coil. Components of the electric field in the plane of the film produce ohmic currents, which deposit thermal energy in the film [19], [20]. The resulting local temperature increase can be detected remotely with an infrared (IR) camera, and from it, the local electric field can be inferred. In this

Manuscript received March 7, 2005; revised October 9, 2005. *Asterisk indicates corresponding author.*

*T. S. Ibrahim is with the Department of Radiology, University of Pittsburgh, Pittsburgh, PA 15216 USA, (e-mail: tsi2@pitt.edu), and also with the School of Electrical and Computer Engineering and Bioengineering Center, University of Oklahoma, Norman, OK 73019 USA.

R. Lee is with the Department of Electrical and Computer Engineering, Ohio State University, Columbus, OH 43210 USA.

Digital Object Identifier 10.1109/TBME.2006.871892